DIC identification and X-FEM simulation of fatigue crack growth based on the Williams' series

C. Roux-Langlois, A. Gravouil, M.-C. Baietto, Julien Réthoré, F. Mathieu, François Hild, Stéphane Roux

International Journal of Solids and Structures 53 (2015) 38–47

Contents lists available at ScienceDirect

International Journal of Solids and Structures

journal homepage: www.elsevier.com/locate/ijsolstr

DIC identification and X-FEM simulation of fatigue crack growth based on the Williams' series

C. Roux-Langlois [a], A. Gravouil [a,b,*], M.-C. Baietto [a], J. Réthoré [a], F. Mathieu [c], F. Hild [c], S. Roux [c]

[a] Laboratoire de Mécanique des Contacts et des Structures (LaMCoS), INSA-Lyon, CNRS (UMR5259), PRES Université de Lyon, Villeurbanne, France
[b] Institut Universitaire de France, France
[c] Laboratoire de Mécanique et Technologie (LMT-Cachan), ENS Cachan, CNRS (UMR8535), PRES UniverSud Paris, Cachan, France

ARTICLE INFO

Article history:
Received 19 January 2014
Received in revised form 23 October 2014
Available online 4 November 2014

Keywords:
Digital Image Correlation (DIC)
Extended finite element method (X-FEM)
Paris' law
Williams' series

ABSTRACT

A unified Digital Image Correlation (DIC)/eXtended Finite Element Method (X-FEM) framework based on the Williams' series for fatigue crack growth identification and simulation is proposed. Williams' series are used for post-processing the displacement measured by digital image correlation. It gives access to the change of stress intensity factors and crack length with the number of cycles. A Paris' crack propagation law is subsequently identified and further validated by simulating the experiment. The simulation uses measured displacements as Dirichlet boundary conditions and a direct estimation of stress intensity factors based on a coupling between a finite element model and the analytical Williams' solutions. It is shown that the use of actual boundary conditions is crucial. The use of the Williams' formalism is further investigated on an elasto-plastic simulation to validate the extraction of nonlinear features in the crack tip vicinity.

1. Introduction

Fracture mechanics concepts (Muskhelishvili, 1953; Williams, 1957; Irwin, 1957) are often used in the study of fatigue crack propagation (Newman, 1998). The stress intensity factors (SIFs), introduced by Irwin (1957) are the leading parameters to characterize the three modes of fracture. They result from the asymptotic study of an infinite 2D elastic medium containing a semi-infinite planar crack using the Williams' series (Muskhelishvili, 1953; Williams, 1957). Situations of small scale yielding where crack growth is mainly controlled by the elastic Williams' coefficients (Suresh, 1998) are often met in high cycle fatigue. For instance, numerous fatigue crack growth laws based on the SIF range have been used (Paris et al., 1961; Molent et al., 2006), or on a similar parameter (McEvily and Illg, 1958). Other Williams' series coefficients play an important role in fatigue and fracture. Numerous crack propagation laws based on these asymptotic coefficients have proven effective (Paris et al., 1961; Suresh, 1998; Hutař et al., 2004; Bathias and Pineau, 2013). The aim of the present study is to provide a methodology for the identification of such fatigue crack growth laws based on the intimate coupling of experimental data (through digital surface imaging) and numerical simulations.

The SIFs identification from experimental data provides a sound basis for describing the propagation of long cracks. The first step is to determine the experimental crack geometry. The main difficulty is to estimate the crack length or the position of the tip. Methods based on electrical potential (Ritchie et al., 1971) or compliance variations (Saxena and Hudak, 1978) require specific equipment, which is mostly applicable to mode I cracks. Most of the marking methods for *post-mortem* analyses impact the propagation speed. Even on pictures of the surface, the crack is only visible once the opening reaches the pixel size, therefore extrapolation methods have been developed. The second step is to determine the SIFs. With the experimental geometry and loading, a classical method is to perform linear elastic simulations. From these simulations, the SIFs are calculated using contour integrals of mechanical fields, either the *J*-integral (Rice, 1968) related to the energy release rate, or interaction integrals (Stern et al., 1976) uncoupling cracking modes. These contour integrals have been transformed into domain integrals to yield more reliable values (Moran and Shih, 1987). To avoid these simulations the chosen experiment has a

* Corresponding author at: Laboratoire de Mécanique des Contacts et des Structures (LaMCoS), INSA-Lyon, CNRS (UMR5259), PRES Université de Lyon, Villeurbanne, France. Tel.: +33 4 72 43 64 25; fax: +33 4 72 43 89 13.

E-mail addresses: clement.roux@insa-lyon.fr (C. Roux-Langlois), anthony.gravouil@insa-lyon.fr (A. Gravouil), marie-christine.baietto@insa-lyon.fr (M.-C. Baietto), julien.rethore@insa-lyon.fr (J. Réthoré), florent.mathieu@lmt.ens-cachan.fr (F. Mathieu), francois.hild@lmt.ens-cachan.fr (F. Hild), stephane.roux@lmt.ens-cachan.fr (S. Roux).

http://dx.doi.org/10.1016/j.ijsolstr.2014.10.026
0020-7683/

simple configuration for which closed-form solutions exist (Broek, 1989). Yet these configurations (especially the boundary conditions) can be challenging to match during the experiment.

The displacement field can be measured by Digital Image Correlation (DIC), be it local (i.e., sub-image based) (Sutton et al., 1983; Sutton et al., 2009) or global (e.g., finite element based) (Besnard et al., 2006; Réthoré et al., 2007). As it gives access to the entire displacement field and not only crack openings, this analysis opens the way to very accurate determinations of crack features. If the displacement field is measured in the vicinity of the crack tip, it is also possible to calculate domain integrals of mechanical fields (Réthoré et al., 2005; Réthoré et al., 2008). The specific displacement bases arising from fracture mechanics analyses can be used to accurately determine the SIFs. McNeill et al. (1987) proposed a least squares projection of the displacement on the singular mode. The projection on a truncation of the Williams' basis developed by Roux and Hild (2006), Roux et al. (2009) accurately provides the corresponding coefficients. Resorting to the Williams' series as a displacement basis allows for the direct evaluation of a small set of generalized degrees of freedom with very low levels of uncertainty. The first super-singular term of the Williams' series can be used to automatically and accurately determine the crack tip position (Hamam et al., 2007; Roux et al., 2009). Higher order super-singular terms are activated by the nonlinearities in the process zone (Hui and Ruina, 1995; Hamam et al., 2007; Roux et al., 2009). The displacement fields can also be used to detect crack closure (Sutton et al., 1999; Sutton et al., 2000; Hamam et al., 2007; Limodin et al., 2009; Carroll et al., 2009), which impacts directly the propagation conditions under cyclic loading when the load ratio is low.

The fracture parameters of the identified propagation law have to be evaluated in the simulations too. Their estimation can also be carried out thanks to strategies based on the Williams' series. This approach avoids the use of post-processing techniques, such as the integral methods, to numerically evaluate the SIFs. A strategy based on the partition of unity method (Babuška and Melenk, 1997) has been introduced (Liu et al., 2004), with one degree of freedom for each asymptotic coefficient. However, it is not accurate to evaluate higher order terms, even if the regular finite element shape functions are not activated in the extraction zone (Xiao and Karihaloo, 2003). Earlier, Tong et al. (1973) proposed the hybrid crack element as an enrichment technique. From this strategy, Karihaloo and Xiao (2001) proposed an accurate evaluation of SIFs and higher order terms. Recently, the hybrid analytical and extended finite element method (HAX-FEM) has been proposed (Réthoré et al., 2010) to couple an analytical model based on a truncated Williams' series expansion in the vicinity of the crack tip with an X-FEM modeling. The coupling was performed using an energetic approach over an overlapping zone (i.e., Arlequin method (Dhia and Rateau, 2005)). The method used herein is very similar to the latter apart from the fact that the coupling is performed on an interface in a weak sense with no overlapping (Passieux et al., 2010; Passieux et al., 2013). It is referred to as DEK-FEM for *Direct Estimation of generalized stress intensity factors K Finite Element Method*.

Even if the SIFs and crack tip positions have been estimated at different stages of propagation, the identification of the crack growth law is far from trivial. The dependence of the crack law coefficients on the set of measurements is strongly nonlinear, and moreover, the measurements themselves are correlated. The computation of crack increments will add further (anti-)correlations in the data series. Resorting to a log scale, albeit natural for a power-law expression, adds up a further distortion to the uncertainty, and implicit weighting of the data for a regression. A critical analysis of these identification procedures led to the formulation of a protocol based solely on DIC measurements, through integrated techniques (Mathieu et al., 2013).

The present study aims at introducing a novel procedure, whereby a first identification of the crack growth law is obtained from the direct determination of the SIF and crack tip position from the DIC displacement field (in the spirit comparable to previous studies (Mathieu et al., 2012)). Then, the DEK-FEM is used to compute the stress intensity factors from the DIC-measured displacements far from the crack tip, used as Dirichlet boundary conditions. This result offers a first validation of the consistency of the measured displacements, SIF and crack tip location. Furthermore, using the crack growth law and remote Dirichlet boundary conditions the simulation provides a prediction of the crack tip position versus time. The procedure is sketched in Fig. 1. It allows the numerical model to closely conform to the experiment. This comparison gives access to a full validation of the procedure. Such a complete and intimate comparison between experimental data and crack growth simulation is the key ingredient of the novel strategy proposed herein. It allows for analyzing an experiment by extracting the fracture parameters and identifying the propagation law from the actual solicitation experienced by the crack. Therefore, the influence of any bias inherent to experimental mechanics (e.g., dissymmetry, mis-orientation) is avoided and the identified parameters become intrinsic material properties. Moreover, the fact that both DIC post-processing and DEK-FEM simulations use the Williams' series decomposition is to be emphasized. It ensures a full consistency in the descriptive language of the sought parameters. Let us also stress that although a Paris' propagation law is identified herein, the strategy can be applied to mixed-mode propagation with a crack growth law based on any subsingular Williams' coefficients (e.g., *T*-stress). The ability

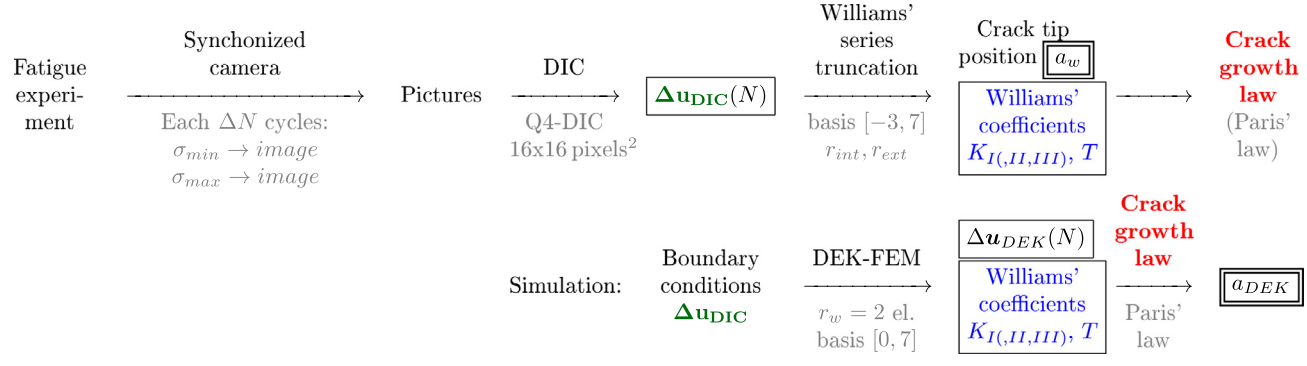

Fig. 1. The different steps of the proposed identification and validation strategy. The DIC procedure evaluates the displacement field from the minimum to the maximum load at the current stage (*N*th cycle) of the fatigue test.

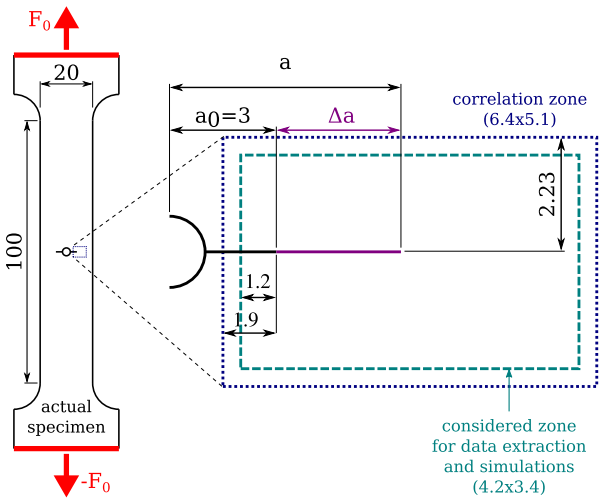

Fig. 2. Geometry (dimension in mm) and boundary conditions of the CCT sample. The correlation area is shown as a thick dotted line. The simulation domain is delineated by the thick dashed line.

of Williams' formalism to extract nonlinear crack features will be illustrated through the analysis of a idealized elasto-plastic simulation.

The outline of the manuscript is as follows. Section 2 presents the considered Center Crack Tension (CCT) test shown in Fig. 2. The chosen parameters are displayed in gray in Fig. 1. An experimental post-processing procedure based on the Williams' series expansion that provides the asymptotic coefficients and the crack tip position is also presented. The DEK-FEM linear elastic simulation approach is discussed in Section 3. In Section 4, both strategies are applied jointly to identify and validate an accurate Paris' fatigue crack growth law.

2. Experimental case study and methods

2.1. Fatigue test on a CCT specimen

The experiment considered hereafter is described in Ref. Mathieu et al. (2012). The specimen is made of commercially pure titanium T35 (max 0.2 wt.% Fe, max 0.18 wt.% O, max 0.08 wt.% C, max 0.03 wt.% N, max 0.015 wt.% H), of yield stress $\sigma_y = 210$ MPa, Young's modulus $E = 100$ GPa, Poisson's ratio $\nu = 0.33$. The specimen geometry is shown in Fig. 2, its thickness is $t = 0.3$ mm, thus a plane stress state is considered. The CCT configuration is a mode I fatigue test where the specimen contains an initially centered small crack perpendicular to the tensile axis. The initial half-crack length a_0 is 3 mm out of a sample half-width W of 10 mm, and the crack grows to reach $a_f = 6$ mm. This sample is subjected to cyclic tensile loading of frequency 10 Hz, from $F_0 = 50$ to 500 N.

During the experiment, both tips at each end of the initial notch are propagating. As shown in Fig. 2, the pictures that will be used for DIC analyses are focused around one crack tip only (i.e., 6.4×5.1 mm^2, see Fig. 4) for high spatial resolution. The propagation is observed between 61,000 cycles and 120,000 cycles. Pairs of pictures are taken each $\Delta N = 1000$ cycles, one at the maximum and one at the minimum load level.

The load ratio R, the load frequency and the environment are kept constant. As illustrated in Ref. Mathieu et al. (2012) for cycle 90,000, a zone of ΔK_I dominance exists, thus the small scale yielding hypothesis applies (Suresh, 1998), ΔK_I is the parameter driving the propagation, and a Paris' law is expected to be relevant for this experiment (Ciavarella et al., 2008). This condition also legitimates the use of an asymptotic series expansion based on a linear elastic model (provided the crack tip region is discarded from the analysis).

2.2. Quantitative kinematics and geometry determination

Digital image correlation (DIC) is a full-field method providing measurements of the displacement and geometry. From two consecutive images seen as scalar (gray level) fields, f at minimum load level and g at the maximum level, the principle used to evaluate the displacement field is the conservation of brightness $f(\boldsymbol{x}) = g(\boldsymbol{x} + \Delta\boldsymbol{u}(\boldsymbol{x})) + b(\boldsymbol{x})$ where $\Delta\boldsymbol{u}$ is the sought displacement field and b acquisition noise. DIC involves solving a nonlinear inverse problem where displacements are spatially interpolated. In the following, the displacement field is decomposed over a regular mesh of finite elements (i.e., four noded quadrangles of size 16×16 pixels, or Q4-DIC (Besnard et al., 2006)). Therefore, a continuous displacement field is provided by the method. Ideally the correlation residual $f(\boldsymbol{x}) - g(\boldsymbol{x} + \Delta\boldsymbol{u}(\boldsymbol{x}))$ consists exclusively of noise b. However, unexpected features of the transformation, or imperfect convergence, can also be seen in the residual so that it can be used to validate the entire procedure. It can also be used to accurately determine the shape of the crack (Réthoré et al., 2008).

2.2.1. Williams' series

A straight crack in an infinite linear elastic two-dimensional domain is considered. The compatible stress and displacement fields are derived around the crack tip (Williams, 1957) and expressed in a polar coordinate system defined in Fig. 3. The stress and displacement fields take the form of a symmetric (mode I) and an anti-symmetric (mode II) series

$$\boldsymbol{\sigma}(r,\theta) = \sum_{n=-\infty}^{\infty} b_I^n r^{n/2-1} \boldsymbol{\psi}_I^n(\theta) + b_{II}^n r^{n/2-1} \boldsymbol{\psi}_{II}^n(\theta) \quad \text{and}$$
$$\boldsymbol{u}(r,\theta) = \sum_{n=-\infty}^{\infty} b_I^n r^{n/2} \boldsymbol{\phi}_I^n(\theta) + b_{II}^n r^{n/2} \boldsymbol{\phi}_{II}^n(\theta). \tag{1}$$

b_I^n and b_{II}^n are the asymptotic coefficients (or Williams' coefficients) depending on boundary conditions.

The terms for $n < 0$ are generally discarded in linear elastic analyses as they would induce an infinite strain energy density at the crack tip. In the vicinity of the crack tip, for a linear elastic medium, the rigid body translations $n = 0$, the SIFs (singular stress $n = 1$), the T-stress (uniform stress) and rotation (both described by $n = 2$) provide a good approximation of the mechanical fields. However, when nonlinearity occurs (e.g., at the post-processing stage), the crack tip position is not known and the first supersingular term i.e., $n = -1$ is used to extract the position associated with the "equivalent elastic medium", see Section 2. Furthermore, when plasticity occurs the supersingular terms are activated (Hui and Ruina, 1995; Hamam et al., 2007; Henninger et al., 2010).

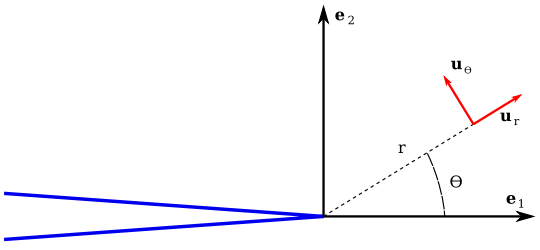

Fig. 3. Local coordinate system around the crack tip.

2.2.2. DIC measurement of Williams' amplitudes and crack tip position

The post-processing method consists of projecting (in the least squares sense) the measured Q4-DIC displacement range onto a truncated Williams' basis (McNeill et al., 1987; Roux and Hild, 2006) to provide the range of Williams' amplitudes and the crack tip position (Hamam et al., 2007; Roux et al., 2009). These data can then be used to identify the fatigue crack growth law.

To have a uniform data treatment for a series of images (as the crack propagates) the projection area shown in Fig. 4 has a constant geometry and moves together with the crack tip. The domain outside a circle of radius r_{ext} is excluded. The radius r_{ext} is chosen as large as possible to maximize the information content and hence minimize the sensitivity to measurement uncertainties. Similarly, a disk of radius r_{int} centered on the crack tip where the plastic strain is expected to be intense is excluded from the analysis (Réthoré et al., 2011). Finally, a thick layer around the crack path is also excluded because of the use of continuous finite elements and the accumulated plastic strain left in the wake of the propagating crack. This final exclusion zone can be seen as the trail of the inner disk as the crack propagates.

Practice has shown (Henninger et al., 2010; Mathieu et al., 2012) that $n_{min} = -3$ and $n_{max} = 7$ allow for an accurate evaluation of the sought Williams' series coefficients (i.e., low order ones such as the SIF)

$$\boldsymbol{u}(r,\theta) = \sum_{i=I,II} \left[\underbrace{\sum_{n_{min}}^{-1} b_i^n \boldsymbol{\phi}_i^n(\theta)\, r^{\frac{n}{2}}}_{\text{"supersingular" terms}} + \underbrace{b_i^0 \boldsymbol{\phi}_i^0}_{\text{translations}} + \underbrace{b_i^1 \boldsymbol{\phi}_i^1(\theta)\sqrt{r}}_{\text{singular term}} + \underbrace{\sum_{n=2}^{n_{max}} b_i^n \boldsymbol{\phi}_i^n(\theta)\, r^{\frac{n}{2}}}_{\text{"subsingular" terms}} \right]. \quad (2)$$

The remote boundary conditions are accounted for by adding higher order terms (Hamam et al., 2007). The so-called supersingular terms (i.e., $n < 0$) are also activated since nonlinearities are expected in a small crack tip region (Hui and Ruina, 1995; Roux et al., 2009). The amplitude of these supersingular terms provide the necessary data to estimate the crack tip location (Roux et al., 2009; Henninger et al., 2010; Mathieu et al., 2012).

To express the Williams' series expansion (i.e., determine r and θ), the crack mouth and tip have to be determined. The crack path location and orientation are usually easy to extract from the displacement field or the correlation residual. In contrast, the crack tip position, which strongly influences the identification of the coefficients of Williams' series expansion (Roux et al., 2009), is more difficult to determine from images when the crack opening has sub-pixel levels. The amplitude b_I^{-1} of the first supersingular field is evaluated and is canceled out by moving the crack tip from the current position to d

$$d = \frac{2\,\tilde{b}_I^{-1}}{\tilde{b}_I^{1}}. \quad (3)$$

A few iterations are generally needed to reach a position where the remaining mis-positioning $d \approx 0$.

In the studied example, the projection of the experimental displacement onto the considered kinematic basis has an RMS difference with the experimental displacement well below 1 pixel (i.e., $< 10^{-1}$ pixel). The crack tip position, a_W, will be used in DEK-FEM simulations (Section 4.3) to combine the experimental approach and the numerical simulation in a consistent way.

2.3. Influence of plasticity

In order to validate the linear elastic approximation of the Williams' series based post-processing, a realistic elastoplastic simulation of the experiment is performed. The considered projection procedure is also validated on this artificial case as all information is readily accessible. In particular, the ability of the supersingular terms to describe the nonlinear phenomena of the process zone, as initially suggested by Hui and Ruina (1995), will be quantified. The superscript s_y refers to the values directly provided by the plastic simulation. The output data are the displacement fields, $\boldsymbol{u}^{s_y}_{min}$ and $\boldsymbol{u}^{s_y}_{max}$ under minimum and maximum load respectively, the incremental and accumulated plastic strain fields and their support. The mode I SIF is also extracted for minimum and maximum loading $K_{I^{s_y}_{min}}$ and $K_{I^{s_y}_{max}}$ using the elastoplastic J-integral on a domain excluding the plastic zone (Moran and Shih, 1987).

For symmetry reasons, only one quarter (50×10 mm) of the sample is studied. Uniform cyclic tensile loading σ_0 (i.e., $\sigma_0 = \frac{F_0}{2tW}$) is prescribed and quasi-static assumption is used. Since plasticity is the main nonlinearity, the material model is assumed homogeneous, elastoplastic with linear kinematic hardening (of modulus $E/100$). In the area where plasticity develops around the crack tip, the mesh is refined ($dh^{s_y} = 40$ μm) to ensure that at least 10 elements are present in the yielding zone. The 65 nodes located along $[a_0, a_0 + 2.6]$ mm represent the successive crack tip positions, the crack tip increment being dh^{s_y}. For a given crack tip position three loading cycles are considered to stabilize the yielding area.

A projection zone similar to that shown in Fig. 4 has been used. The inner and outer radii of the main annulus are $r_{int} = 0.8$ mm and $r_{ext} = 2.4$ mm respectively. In addition a strip of width $2r_{int}$ is excluded from the projection zone. The amplitudes b_i^n are estimated from the projection of the displacement field difference $\Delta\boldsymbol{u} = \boldsymbol{u}^{s_y}_{max} - \boldsymbol{u}^{s_y}_{min}$ onto the truncated Williams' series $-3 \leqslant n \leqslant 7$. The crack tip position (see Fig. 5(a)) is accurately determined. This figure displays the crack tip position of the simulation and three evaluations from the projection of the computed displacement fields $\boldsymbol{u}^{s_y}_{min}$, $\boldsymbol{u}^{s_y}_{max}$ and $\Delta\boldsymbol{u}^{s_y} = \boldsymbol{u}^{s_y}_{max} - \boldsymbol{u}^{s_y}_{min}$ onto the Williams' series and canceling out the amplitude b_I^{-1}. The projections of $\boldsymbol{u}^{s_y}_{min}$ and $\boldsymbol{u}^{s_y}_{max}$ lead to overestimations of the crack length. This gap is due to cumulated plasticity. In contrast $\Delta\boldsymbol{u}^{s_y}$ is only mildly affected by plasticity in one loading cycle, as it is very mildly influenced by most of the plastic history. Therefore, the small scale yielding hypothesis, which legitimates the elastic approach, is more likely to be valid when analyzing the $\Delta\boldsymbol{u}$ fields.

Fig. 5(b) compares the SIF amplitude ΔK_I extracted from the projection of $\Delta\boldsymbol{u}^{s_y}$ and Tada's closed-form solution (Tada et al., 1985) with the J-integral measurement $\Delta K_{J^{s_y}} = K_{I^{s_y}_{max}} - K_{I^{s_y}_{min}}$. Tada's solution has been obtained from elastic simulations and deviates from the J-integral measurement by about 1% due to plasticity in the simulation. The SIF amplitude determined by projection is shown to be consistent with $\Delta K_I^{s_y}$. The residual of this projection (from the identified Williams' coefficients in Eq. (2)) has a standard deviation of $10^{-4}\max(\boldsymbol{u}^{s_y})$. Thus the procedure based on the elastic

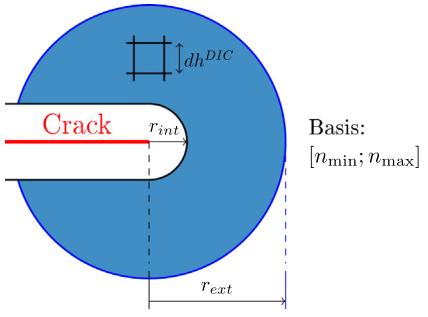

Fig. 4. Parameterized projection area. r_{ext} is the external radius around the crack tip, r_{int} the internal radius, dh^{DIC} the size of Q4-DIC elements, n_{min} and n_{max} the limits of the Williams' series projection basis.

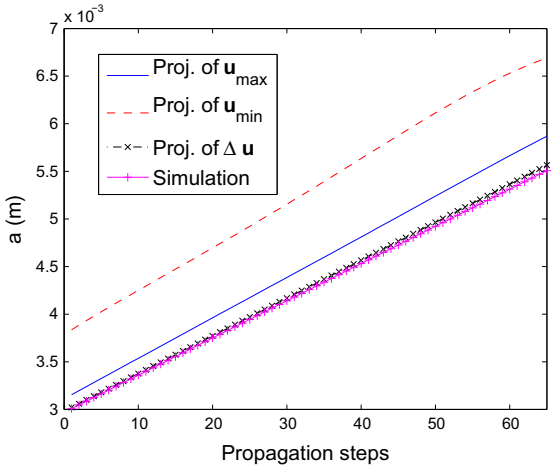

(a) a_W position canceling out b_I^{-1}

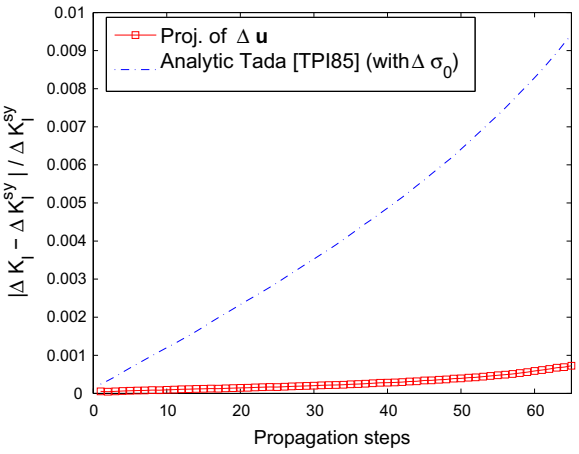

(b) Variation of SIF with J-integral as a reference $|\Delta K_I - \Delta K_I^{s_y}|/\Delta K_I^{s_y}$, (with $\Delta K_I^{s_y} = K_{I\,s_y}^{max} - K_{I\,s_y}^{min}$) for different evaluations of ΔK_I

Fig. 5. Projection of the elastoplastic fields for different propagation increments.

Williams' series expansion is considered as validated even in the case of small scale yielding.

Quantifying nonlinearities is necessary to set the value of r_{int} in the procedure. In the sequel, the evaluation of the monotonic plastic zone size (i.e., under maximum loading (Suresh, 1998)) is studied especially when, as in experiments, the only available information is the measured displacement field. For simple geometries and material behaviors, analytical evaluations of the monotonic process zone ahead of the crack tip (i.e., in the $\boldsymbol{e}_1$ direction) exist (Suresh, 1998). For instance, resorting to a cohesive zone model, Dugdale (1960) proposed $r_y^{DB} = (\pi/8)(K_I/\sigma_y)^2$ where σ_y is the yield stress.

Once the displacement field has been projected onto the Williams' series, an elastic stress field can directly be computed from the estimated Williams' coefficients, see Eq. (1). The process zone shape and size r_y^W are estimated from this stress field using von Mises' criterion with the yield stress σ_y. The shape is shown in Fig. 6(a) for different choices of the projection basis at the maximum load during the first cycle. The subsingular fields play no role as it could have been anticipated since their strain and stress fields vanish at the crack tip. The agreement obtained between the full elastoplastic simulation and the three parameter evaluation obtained from the elastic fields $n = -3$, -1 and 1 and a simple von Mises' criterion is good. To further validate the ability of the procedure to capture a fair estimate of the yield stress, the size of the plastic zone as could be estimated from various possible indicators is shown in Fig. 6(b). These estimates are scaled by the value obtained from the complete elastoplastic simulation ahead of the crack $r_y^{s_y}$, considered here to be the reference $r_y^{ref} = r_y^{s_y}$. The studied estimators of the plastic zone size are:

- r_y^{DB}, the Dugdale estimate (Dugdale, 1960).
- r_y^W, the size obtained by using von Mises' criterion on the elastic field computed from the Williams' series projection.

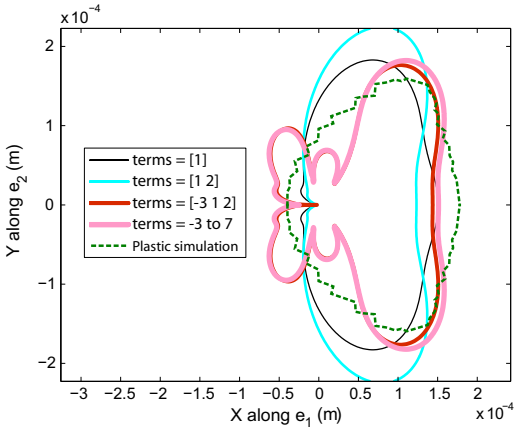

(a) Contour of the area where von Mises' elastic stress (σ_{vM}), computed from the displacement projection, is greater than the yield stress when varying the number of terms of the Williams' series $\boldsymbol{\sigma} = \sum_{n=-\infty}^{\infty} b_I^n r^{n/2-1} \boldsymbol{\psi}_I^n(\theta) + b_{II}^n r^{n/2-1} \boldsymbol{\psi}_{II}^n(\theta)$

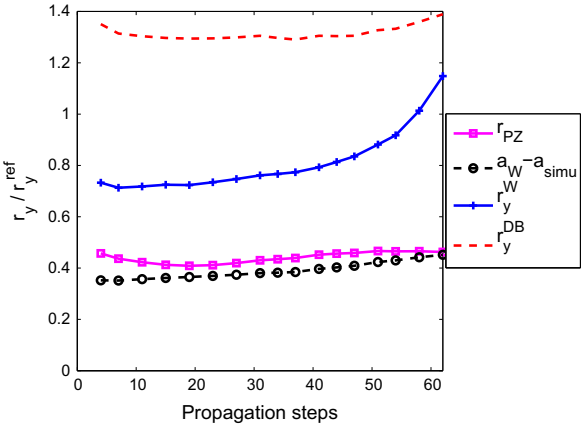

(b) Evaluations of the plastic radius ahead of the crack under maximum load during the propagation normalized by the value in the simulation $r_y^{ref} = r_y^{s_y}$

Fig. 6. Plastic zone size around the crack tip.

- $r_{PZ} = -8\sqrt{b_I^{-3}/b_I^1}$, computed from the Williams' series amplitudes, as proposed (Roux et al., 2009).
- $a_W - a_{simu}$, the distance from the elastic equivalent far field position of the crack tip and the actual one, as their difference is expected to vary in proportion to the plastic radius.

It is worth noting that those estimates remain approximately constant for a significant crack advance. Their precise level can be adjusted from a calibration stage such as the present comparison. r_{PZ} turns out to provide the most stable value among all the other estimators.

3. Numerical modeling strategy DEK-FEM

3.1. Domain decomposition

The proposed simulation strategy is linear elastic and also relies on the Williams' series. Since it directly provides the asymptotic coefficients as degrees of freedom, this strategy is called DEK-FEM (Passieux et al., 2010; Passieux et al., 2013). The domain is decomposed into an X-FEM part and a so-called analytical patch around the crack tip (see Fig. 7). Since, the analytical expansion of the displacement field in the crack tip vicinity is valid for straight cracks, the analytical patch must be small enough to be localized in an area where the crack curvature can be neglected. Therefore, this analytical patch is made compatible with a localized multigrid approach (Passieux et al., 2010).

Let us consider the well-posed problem described in Fig. 7 where displacement boundary conditions are applied on $\partial_1\Omega$ and traction boundary conditions on $\partial_2\Omega$ with $\partial\Omega = \partial_1\Omega \cup \partial_2\Omega$ and $\partial_1\Omega \cap \partial_2\Omega = \varnothing$. The domain Ω is composed of two parts, namely, an "analytical patch", Ω_W, in the vicinity of the crack tip where mechanical fields can be singular and an "outer domain", Ω_X. In the present case, Ω_X is discretized within an X-FEM framework, its associated displacement space is $\mathcal{U}_X$. In practice, once the mesh of domain Ω is chosen, few layers of elements around the crack tip are replaced by the analytical patch Ω_W of radius r_W.

3.2. Crack tip patch and interface

The discretization space $\mathcal{U}_W$ of Ω_W is a truncation of the Williams' series (1) for $n \in [0 \dots n_{DEK}]$. Therefore, the associated degrees of freedom are directly the coefficients b_I^n and b_{II}^n of the Williams' series expansion. To link the two parts of the model, the displacements along a common interface are connected in a weak sense. Compatibility between the displacements is then enforced by Lagrange multipliers $\boldsymbol{\lambda} \in \mathcal{L}$ where $\mathcal{L}$ is an *ad hoc* space (Passieux et al., 2010)

$$\langle \boldsymbol{u}_X - \boldsymbol{u}_W, \boldsymbol{\lambda} \rangle_{\Gamma_W} = \int_{\Gamma_W} \boldsymbol{\lambda} \cdot (\boldsymbol{u}_X - \boldsymbol{u}_W) dS = 0. \tag{4}$$

This integral matching avoids half-enriched elements (often called blending elements) that come from the partition of unity method (Chahine et al., 2011). By comparison with the HAX-FEM (Réthoré et al., 2010) overlapping method, such a matching improves the accuracy of the solution, in particular the SIF evaluation.

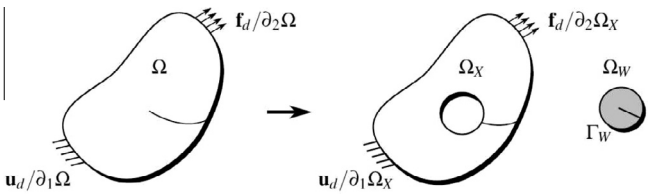

Fig. 7. Domain decomposition between the analytical patch Ω_W and the X-FEM area Ω_X (Passieux et al., 2010).

The analytical domain size r_W and the order of truncation n_{DEK} of series (1) are the two parameters that have to be determined. When higher-order terms (from $n_{DEK} = 5$ on) of the expansion are taken into account, the determination of the SIFs is independent of the increase of the analytical patch dimension. Consequently, the Williams' expansion terms ranging from 0 to $n_{DEK} = 7$ are considered in the analytical patch. A patch size ($r_W = 3dh^{DEK}$) is large enough to display sufficient flexibility (devoid of the constraint of matching the X-FEM kinematic description) to give an accurate evaluation of SIFs (Passieux et al., 2010).

4. Identification and validation of a high cycle fatigue propagation law

The projection of the measured displacement field automatically provides the crack tip position and the Williams' series coefficients including the SIF for each analyzed cycle. A standard Paris' law (Paris et al., 1961) relating crack growth per cycle with the range of the SIF is chosen

$$\frac{da}{dN} = C(\Delta K_I)^{\eta}, \tag{5}$$

where C and η are material-dependent parameters to be identified. In the sequel, the efficiency of the presented identification procedure is analyzed but not the choice of the crack growth law expression. However, it is worth noting that the proposed strategy is not limited to propagation laws based on singular amplitudes (e.g., Δb_I^1). Other asymptotic amplitudes (i.e., $\Delta b_i^n,\ n \in [0, n_{max}]$) are measured and can be used in more sophisticated crack growth laws such as that proposed by Hutař et al. (2004) that involves the T-stress.

Furthermore, other parameters influence the crack propagation such as the load ratio or crack closure. When crack closure occurs, the full-field displacement measurement can be used to directly evaluate effective SIF (Hamam et al., 2007; Carroll et al., 2009). The proposed strategy may be extended to crack closure situations provided enough images are acquired during unloading/reloading cycles to capture crack closure/opening.

4.1. Experimental data evaluation

The above discussed DIC procedure is applied to analyze and simulate the CCT fatigue test presented in Section 2. A set of images (pixel size: 6.1 μm) at minimum and maximum load of fatigue cycles is analyzed. The variations of displacement fields from minimum to maximum load $\Delta\boldsymbol{u}$ is obtained from Q4-DIC (Besnard et al., 2006) as carried out in Refs. Mathieu et al. (2012, 2013), with elements of 16×16 pixels^2. These fields are then projected onto the Williams' series, providing the relevant Williams' amplitudes, Δb_I^n, and, from them, a_W and ΔK_I^{DIC-WA}. This data set is referred to with the acronym DIC-WA (for DIC-Williams' Amplitudes) in the following. The comparison between DIC displacement and DEK-FEM simulation reveals that optical distortions occur at the boundary of the field of view. This allows us to set the region of interest (and r_{ext}). The region of interest is selected as a 4.2×3.4 mm^2 rectangle. The projection domain parameters are $r_{ext} = 2.1$ mm and $r_{int} = 0.6$ mm, and the truncated Williams' series is limited from $n_{min} = -3$ to $n_{max} = 5$.

4.2. Numerical simulation strategies

Three different strategies are used to evaluate the stress intensity factor amplitude ΔK_I over a cycle. The first one is based on a

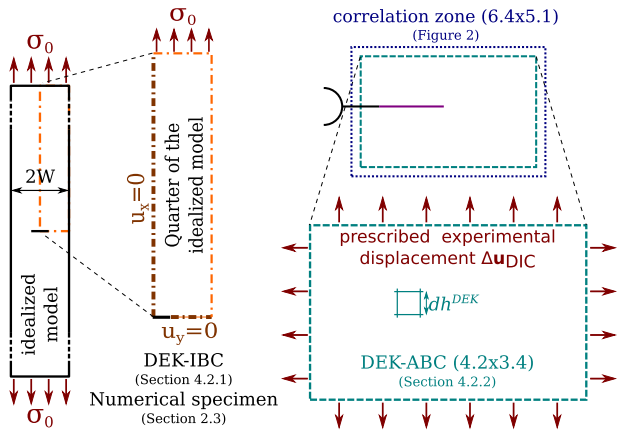

Fig. 8. Geometry and boundary conditions of the sample. The correlation area is represented with its projection zone. Idealized stress boundary conditions or experimental Dirichlet boundary conditions (scale in mm) are prescribed to the simulated systems.

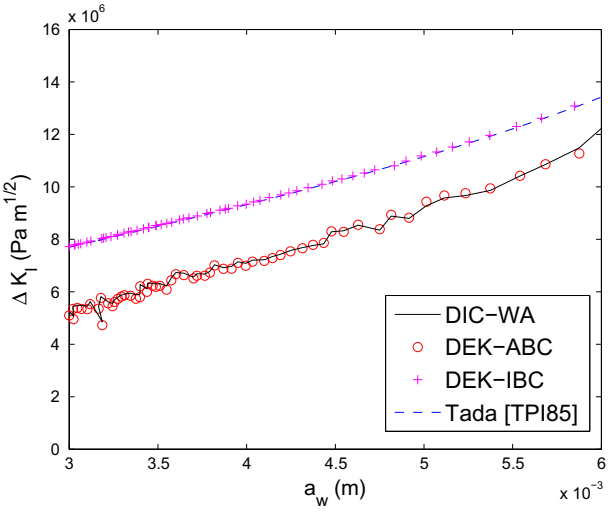

Fig. 9. Comparison between simulation and projection with crack tip located at a_W using different evaluations of ΔK_I.

published reference solution of the ideal test as studied by Tada et al. (1985), the second one is obtained from the above presented numerical modeling using DEK-FEM of the same ideal test, and a third one is based on the same numerical model but uses experimentally measured boundary conditions. In addition to these three evaluations, the Williams' series decomposition of the DIC field also provides a measurement of ΔK_I^{DIC-WA}. These four estimates will be compared.

4.2.1. Ideal test solutions

For the ideal test geometry shown in Fig. 8, under plane stress and uniform tensile loading $\Delta\sigma_0 = \frac{\Delta F_0}{2Wt}$ and elastic behavior, Tada et al. (1985) proposed a closed-form solution for the SIF amplitude

$$\Delta K_I^{Tada} = \Delta\sigma_0\sqrt{\pi a}\left[1 - 0.025\left(\frac{a}{W}\right)^2 + 0.06\left(\frac{a}{W}\right)^4\right]\sqrt{\frac{1}{\cos\left(\frac{\pi a}{2W}\right)}} \qquad (6)$$

Reference to ΔK_I evaluated from this equation will be denoted as "Tada's prediction".

The DEK-FEM numerical approach (Section 3) is used to evaluate ΔK_I from the same loading conditions, geometry and under the same assumptions. Because of symmetry, a quarter of the CCT plate ($(1/4) \times 2W \times 100$) is considered subjected to uniform remote stress $\Delta\sigma_0 = \Delta F_0/2Wt$. Results of this second approach will be referred to as DEK-IBC (for Ideal Boundary Conditions).

4.2.2. DEK-FEM simulation based on DIC analysis

It can be noted that the boundary conditions used in the simulation of the full specimen are an idealization of the actual ones applied experimentally. The main merit of using a consistent description for the experiment and the simulation is to offer the possibility of taking into account the actual boundary conditions as experienced by the specimen, even if they depart from the ideal test (Fedele et al., 2009; Rannou et al., 2010). This is the purpose of this third evaluation.

A DEK-FEM simulation is now performed on a part of the region where the displacements from DIC measurements are available (i.e., DEK-ABC of Fig. 8). On the boundary of that area, the displacement amplitude $\Delta\boldsymbol{u}^{DIC}$ extracted from the DIC measurements is prescribed as Dirichlet boundary conditions. Further, the mesh used for the correlation measurement is fine enough to have an accurate evaluation of SIFs when used in the DEK-FEM simulations (i.e., a mesh four times finer leads to a difference in evaluated SIFs less than 1%). Moreover, having the same mesh for the simulation and the correlation analysis makes the application of boundary conditions easier. This DEK-ABC (for Actual Boundary Conditions) simulation relaxes two hypotheses, namely, the idealized boundary conditions and the symmetric propagation of both crack tips. The first and presumably the second of these two hypotheses are not fulfilled in the experiment.

4.3. Simulations with prescribed experimental crack tip position a_W

First, numerical simulations are run with a prescribed history of crack tip positions extracted by projection of the measured displacement fields onto the Williams' series. The SIFs are computed and compared to experimental estimates. Fig. 9 shows the stress intensity factor as a function of the measured crack tip position. The DEK-FEM simulations using the ideal boundary conditions *DEK − IBC* give stress intensity factors that can hardly be distinguished from Tada's predictions Eq. (6). This agreement shows the accuracy of DEK-FEM simulations and are considered as a validation of the numerical procedure.

Fig. 9 also shows that the DEK-ABC simulations (Section 4.2.2) yield SIFs values $\Delta K_I^{DEK-ABC}$ very close to those obtained with the experimental post-processing procedure (i.e., ΔK_I^{DIC-WA}). This result demonstrates that the assumptions made on the elastic behavior of the sample over the analyzed region are well satisfied, and that the DIC measurement is extremely reliable over the bulk of the region of interest (the boundaries are by construction identical). Projected and simulated displacements have a low RMS difference when compared with the measured displacement fields (i.e., $< 7 \times 10^{-2}$ pixel). This difference is of the order of the measurement uncertainty and thus shows that the Williams' series and DEK-FEM bases accurately describe the experimental displacement fields.

The two previous observations show that the reference solution, the modeling approach and the DIC technique are all consistent with each other. Yet a very significant difference in ΔK_I (i.e., by more than 10%) can be observed in Fig. 9 between Tada'spredictions and DEK-IBC on the one hand, and DEK-ABC and DIC-WA on the other hand. The conclusion to be drawn from these comparisons is that the boundary conditions of the experiment are not consistent with those of an ideal test. Among the different conditions of the ideal test, the assumption of a perfectly symmetric loading appears as the most fragile. Any slight dissymmetry in loading, or initial geometry of the notch, or even its tip curvature, as well as any minute fluctuations in the material properties at the crack tip will induce a breakdown of symmetry that will increase

with further crack growth. This result shows the importance of properly accounting for the actual boundary conditions. In the following, it will be shown that this difference becomes even more striking when a crack growth law is identified.

4.4. Crack growth law identification

The identification can now be performed based on the measured crack length $a(N)$ and SIF amplitude $\Delta K_I(N)$. The procedure followed herein has been introduced in Reference Mathieu et al. (2012). It consists of minimizing $\mathcal{A}$ the time cumulated quadratic difference of the measured and predicted crack lengths. The predicted crack length itself results from the integration of Paris' law $da/dN = C(\Delta K_I(N))^\eta$ computed from the $\Delta K_I(N)$ time series. Explicitly, the objective function to be minimized is

$$\mathcal{A}(C,\eta) = \sum_{p=1}^{N_f} \left[a(N_0) - a(N_p) + \sum_{i\in[2\ldots p]} C \frac{(\Delta K_I(N_{i-1}))^\eta + (\Delta K_I(N_i))^\eta}{2} (N_{i-1} - N_i) \right]^2 \tag{7}$$

where propagation is monitored from N_0 to N_f, at cycles N_p.

From the previous section, it has been shown that due to imperfections in the experiment, or conversely to idealization of actual loading conditions, the local evaluation of ΔK_I does not match the theoretically expected one. Two parameter sets of Paris' crack growth law can thus be identified.The first one considers K_I^{DIC-WA} as representative of the actual boundary conditions (denoted as *ABC – Paris* in the following), while the second one uses the ΔK_I^{Tada} with *ideal* boundary conditions (denoted as *IBC – Paris*). As a consequence of this last result, using solely a careful inspection of the crack tip position but without resorting to full field measurements, it is possible to estimate a Paris' crack growth law (*IBC – Paris*) assuming ideal boundary conditions. The identified parameters are given in Table 1, along with previously published values. A good agreement is observed between the reported results and those obtained herein when the experimentally measured boundary conditions are considered.

Table 1
Identified coefficients for Paris' law compared with previous studies of this experiment (Mathieu et al., 2012; Mathieu et al., 2013), and with values for another titanium grade (Adib and Baptista, 2007). Units such that the crack length a is expressed in mm, and SIF range ΔK_I in MPa$\sqrt{\text{m}}$.

Parameters	10^{11} C	η
IBC – Paris (Mathieu et al., 2013)	0.3	4.4
ABC – Paris	5.3	3.4
Adib and Baptista (2007)	7.5	3.0
Integrated DIC (Mathieu et al., 2012)	4.7	3.1
Fully integrated procedure (Mathieu et al., 2013)	2.5	3.4

4.5. Simulation of propagation

Once the crack propagation law is identified, crack propagation is simulated. The crack tip position is now set to its initial position to start the simulation, and then it is computed from Paris' growth law and computed SIFs values. Integration is explicit in time with a time step of 1000 cycles. The results are shown in Fig. 10 in terms of crack growth as a function of the propagation step. Fig. 10(a) displays the crack tip positions obtained from the simulation DEK-ABC with the two crack propagation laws (*ABC – Paris* and *IBC – Paris*). These simulations are compared to the crack growth predicted by DEK-IBC, which is equivalent to Tada's solutions, according to the two crack propagation laws, as displayed in Fig. 10(b).

The DEK-ABC crack advance(see Fig. 10(a)) agrees well with the experimental measurement Δa_W when the *ABC – Paris* law is used. Even if such a good agreement could have been anticipated because of the identification procedure used, integration of such a strongly nonlinear law may have revealed a residual discrepancy. Thus, it can also be interpreted as the adequacy of the Paris' law algebraic form, together with a reliable identification procedure. The same graph also shows that the *IBC – Paris* law is clearly inconsistent with the experimental results, which is a natural consequence of the previous observation of the differences between DEK-IBC and DEK-ABC SIFs.

Fig. 10(b) shows that the *IBC – Paris* law in DEK-IBC simulations predicts a crack position that fits very well the experimental data. The regression quality is quite comparable to what was obtained for *ABC – Paris* law used in simulation and DIC-WA data shown in Fig. 10(a). From Figs. 9 and 10(a), it is observed that idealized boundary conditions may lead to bad SIF evaluations and then to overestimate the crack advance. Identification resorting to full-field displacement measurement allows the identification of the SIF and then of the *ABC – Paris* crack growth law without assumption on the boundary conditions.

Furthermore, it provides an assessment of the simulation model through to the comparison between experimental full-field

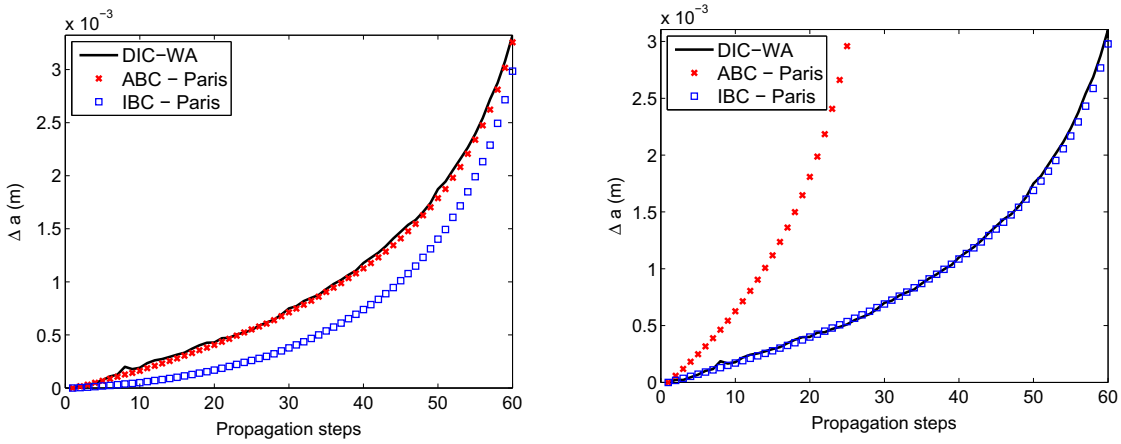

(a) DEK-FEM simulation close to the crack tip with measured boundary conditions (DEK-ABC)

(b) Simulation of the full specimen with ideal boundary conditions (DEK-IBC equivalent to Tada's prediction)

Fig. 10. Comparison of the different propagation velocities with full and crack tip vicinity simulations.

displacement measurements and simulated displacement fields. From Fig. 10(b), the influence of boundary conditions in crack propagation simulation observed in Ref. Rannou et al. (2010) is displayed. The assumption of idealized boundary conditions in the simulation with the *ABC – Paris* law leads to an underestimation of the crack advance by a factor of 3 to 4. The assumption of idealized boundary conditions is thus problematic when it is not accounted for both in the crack growth law identification and simulations. However, the *IBC – Paris* law may include experimental biases leading to higher SIF range values. The identified Paris'law coefficient may thus exhibit a large scatter between different tests and/or experimental devices or operators. It is not the case for the *ABC – Paris* law that considers the actual loading conditions of the specimen.

From the above analysis it is concluded that identifying an accurate crack growth law cannot rely on globally approximated boundary conditions. It was shown herein that this is one of the key points of a fatigue crack growth law identification and of its validation through propagation simulations. A method based on Q4-DIC displacement measurement, SIFs estimations based on the Williams' series and simulations using experimentally measured boundary conditions and a Williams' patch around the crack tip has been validated. The consistent framework of analysis used for the DIC analysis and FEM simulations revealed not only convenient, but also very instrumental for reaching trustful conclusions.

5. Conclusion

A new strategy to accurately identify and simulate fatigue crack propagation is presented herein. It unifies experimental full-field measurements and numerical simulations. Both approaches are based on a truncation of the Williams' series expansion, giving access to asymptotic coefficients such as the stress intensity factors, *T*-stress from the experiment and provided by the simulation (and, for the experimental analysis, a similar treatment for the supersingular amplitude provides the crack tip position). This formalism is used in conjunction with DIC analyses of the displacement field, and a recently proposed extended X-FEM strategy, where a similar enrichment is proposed over a patch around the crack tip. The parallel is all the more complete that the boundary conditions prescribed in the X-FEM simulation are the measured experimental displacement fields.

This procedure was used to identify parameters of the Paris' law for the crack growth in a CCT cyclic fatigue test performed on a thin titanium sheet. The numerical simulation of the crack growth using the DEK-FEM numerical model and a time integration of the Paris' law was shown to accurately reproduce the observed crack advance. It was shown that a comparable procedure could be followed based on the assumption of an ideal test. A different Paris' law would result in a similar agreement with the observed crack advance, when a similar ideal loading is considered. One important observation of the present study is that any slight imperfection in the actual experimental test may lead to very strong errors in crack length predictions, errors that cannot be detected from the crack tip position history (when a consistent assumption on loading is made).

Having a homogeneous toolbox for analyzing and modeling the experimental test allows unavoidable imperfections and breakdown of symmetries to be accounted for. Securing the actual boundary conditions of the test in the analysis as well as in the modeling, allows for the identification of crack growth laws with a much improved reliability. Let us finally stress the generality of the proposed procedure, as no closed-form of asymptotic coefficients are needed, and any geometry and loading can be considered.

Acknowledgments

This work has been supported by the French National Research Agency (Grant ANR-09-BLAN-0009-01-RUPXCUBE).

Appendix A. Supplementary data

Supplementary data associated with this article can be found, in the online version, at http://dx.doi.org/10.1016/j.ijsolstr.2014.10.026.

References

Adib, A.M.L., Baptista, C.A.R.P., 2007. An exponential equation of fatigue crack growth in titanium. Mater. Sci. Eng. A 452–453, 321–325.
Babuška, I., Melenk, J., 1997. The partition of unity method. Int. J. Numer. Methods Eng. 40, 727–758.
Bathias, C., Pineau, A., 2013. Fatigue of Materials and Structures: Application to Damage and Design. ISTE, Wiley.
Besnard, G., Hild, F., Roux, S., 2006. Finite-element displacement fields analysis from digital images: application to Portevin-Le Châtelier bands. Exp. Mech. 46, 789–804.
Broek, D., 1989. The Practical Use of Fracture Mechanics. Springer, Netherlands.
Carroll, J., Efstathiou, C., Lambros, J., Sehitoglu, H., Hauber, B., Spottswood, S., Chona, R., 2009. Investigation of fatigue crack closure using multiscale image correlation experiments. Eng. Fract. Mech. 76 (15), 2384–2398.
Chahine, E., Laborde, P., Renard, Y., 2011. A non-conformal eXtended finite element approach: integral matching XFEM. Appl. Numer. Math. 61 (3), 322–343.
Ciavarella, M., Paggi, M., Carpinteri, A., 2008. One, no one, and one hundred thousand crack propagation laws: a generalized Barenblatt and Botvina dimensional analysis approach to fatigue crack growth. J. Mech. Phys. Solids 56 (12), 3416–3432.
Dhia, H.B., Rateau, G., 2005. The Arlequin method as a flexible engineering design tool. Int. J. Numer. Methods Eng. 62 (11), 1442–1462.
Dugdale, D.S., 1960. Yielding of steel sheets containing slits. J. Mech. Phys. Solids 8, 100–104.
Fedele, R., Raka, B., Hild, F., Roux, S., 2009. Identification of adhesive properties in glare assemblies using digital image correlation. J. Mech. Phys. Solids 57 (7), 1003–1016.
Hamam, R., Hild, F., Roux, S., 2007. Stress intensity factor gauging by digital image correlation: application in cyclic fatigue. Strain 43 (3), 181–192.
Henninger, C., Roux, S., Hild, F., 2010. Enriched kinematic fields of cracked structures. Int. J. Solids Struct. 47 (24), 3305–3316.
Hui, C.Y., Ruina, A., 1995. Why k? High order singularities and small scale yielding. Int. J. Fract. 72 (2), 97–120.
Hutař, P., Seitl, S., Knésl, Z., 2004. Quantification of the effect of specimen geometry on the fatigue crack growth response by two-parameter fracture mechanics. Mater. Sci. Eng. A 387–389, 491–494.
Irwin, G.R., 1957. Analysis of stresses and strains near the end of a crack traversing a plate. J. Appl. Mech. 24, 361–364.
Karihaloo, B.L., Xiao, Q.Z., 2001. Accurate determination of the coefficients of elastic crack tip asymptotic field by a hybrid crack element with p-adaptivity. Eng. Fract. Mech. 68 (15), 1609–1630.
Limodin, N., Réthoré, J., Buffière, J.-Y., Gravouil, A., Hild, F., Roux, S., 2009. Crack closure and stress intensity factor measurements in nodular graphite cast iron using three-dimensional correlation of laboratory X-ray microtomography images. Acta Mater. 57 (14), 4090–4101.
Liu, X.Y., Xiao, Q.Z., Karihaloo, B.L., 2004. XFEM for direct evaluation of mixed mode SIFs in homogeneous and bi-materials. Int. J. Numer. Methods Eng. 59 (8), 1103–1118.
Mathieu, F., Hild, F., Roux, S., 2012. Identification of a crack propagation law by digital image correlation. Int. J. Fatigue 36 (1), 146–154.
Mathieu, F., Hild, F., Roux, S., 2013. Image-based identification procedure of a crack propagation law. Eng. Fract. Mech. 103, 48–59.
McEvily, A.J. Jr., Illg, W., 1958. The rate of fatigue crack propagation in two aluminum alloys. Technical Note 4394, NACA.
McNeill, S.R., Peters, W.H., Sutton, M.A., 1987. Estimation of stress intensity factor by digital image correlation. Eng. Fract. Mech. 28 (1), 101–112.
Molent, L., Jones, R., Barter, S., Pitt, S., 2006. Recent developments in fatigue crack growth assessment. Int. J. Fatigue 28 (12), 1759–1768.
Moran, B., Shih, C.F., 1987. Crack tip and associated domain integrals from momentum and energy balance. Eng. Fract. Mech. 27 (6), 615–642.
Muskhelishvili, N.I., 1953. Some Basic Problems of the Mathematical Theory of Elasticity.
Newman Jr., J.C., 1998. The merging of fatigue and fracture mechanics concepts: a historical perspective. Prog. Aerosp. Sci. 34 (5), 347–390.
Paris, P., Gomez, M., Anderson, W., 1961. A rational analytic theory of fatigue. Trend Eng. 13, 9–14.
Passieux, J.-C., Gravouil, A., Réthoré, J., Baietto, M.-C., 2010. Direct estimation of generalized stress intensity factors using a three-scale concurrent multigrid X-FEM. Int. J. Numer. Methods Eng. 85 (13), 1648–1666.

Passieux, J.-C., Réthoré, J., Gravouil, A., Baietto, M.-C., 2013. Local/global non-intrusive crack propagation simulation using a multigrid X-FEM solver. Comput. Mech. 52 (6), 1381–1393.
Rannou, J., Limodin, N., Réthoré, J., Gravouil, A., Ludwig, A., Baietto-Dubourg, M.C., Buffière, J.Y., Combescure, A., Hild, F., Roux, S., 2010. Three dimensional experimental and numerical multiscale analysis of a fatigue crack. Comput. Methods Appl. Mech. Eng. 199 (21–22), 1307–1325 (Multiscale Models and Mathematical Aspects in Solid and Fluid Mechanics).
Réthoré, J., Gravouil, A., Morestin, F., Combescure, A., 2005. Estimation of mixed-mode stress intensity factors using digital image correlation and an interaction integral. Int. J. Fract. 132, 65–79.
Réthoré, J., Roux, S., Hild, F., 2007. From pictures to extended finite elements: extended digital image correlation (X-DIC). C. R. Mécanique 335 (3), 131–137.
Réthoré, J., Hild, F., Roux, S., 2008. Extended digital image correlation with crack shape optimization. Int. J. Numer. Methods Eng. 73, 248–272.
Réthoré, J., Roux, S., Hild, F., 2008. Noise-robust stress intensity factor determination from kinematic field measurements. Eng. Fract. Mech. 75 (13), 3763–3781.
Réthoré, J., Roux, S., Hild, F., 2010. Hybrid analytical and extended finite element method (HAX-FEM): a new enrichment procedure for cracked solids. Int. J. Numer. Methods Eng. 81 (3), 269–285.
Réthoré, J., Roux, S., Hild, F., 2011. Optimal and noise-robust extraction of fracture mechanics parameters from kinematic measurements. Eng. Fract. Mech. 78 (9), 1827–1845.
Rice, J.R., 1968. A path independent integral and the approximate analysis of strain concentration by notches and cracks. J. Appl. Mech. 35, 379–386.
Ritchie, R.O., Garrett, G.G., Knott, J.P., 1971. Crack-growth monitoring: optimisation of the electrical potential technique using an analogue method. Int. J. Fract. 7 (4), 462.
Roux, S., Hild, F., 2006. Stress intensity factor measurements from digital image correlation: post-processing and integrated approaches. Int. J. Fract. 140 (1–4), 141–157.
Roux, S., Réthoré, J., Hild, F., 2009. Digital image correlation and fracture: an advanced technique for estimating stress intensity factors of 2D and 3D cracks. J. Phys. D Appl. Phys. 42 (214004).
Saxena, A., Hudak Jr., S.J., 1978. Review and extension of compliance information for common crack growth specimens. Int. J. Fract. 14 (5), 453–468.
Stern, M., Becker, E.B., Dunham, R.S., 1976. A contour integral computation of mixed-mode stress intensity factors. Int. J. Fract. 12, 359–368.
Suresh, S., 1998. Fatigue of Materials. Cambridge Solid State Science Series. Cambridge University Press.
Sutton, M.A., Wolters, W.J., Peters, W.H., Ranson, W.F., McNeill, S.R., 1983. Determination of displacements using an improved digital correlation method. Image Vision Comput. 1 (3), 133–139.
Sutton, M.A., Zhao, W., McNeill, S.R., Helm, J.D., Piascik, R.S., Riddell, W.T., 1999. Local crack closure measurements: development of a measurement system using computer vision and a far-field microscope. ASTM Spec. Tech. Publ. 1343, 145–156.
Sutton, M.A., McNeill, S.R., Helm, J.D., Chao, Y.J., 2000. Advances in two-dimensional and three-dimensional computer vision. In: Rastogi, P.K. (Ed.), Photomechanics: Topics in Applied Physics, vol. 77. Springer, Berlin Heidelberg, pp. 323–372.
Sutton, M.A., Orteu, J.J., Schreier, H., 2009. Image Correlation for Shape, Motion and Deformation Measurements: Basic Concepts, Theory and Applications. Springer.
Tada, H., Paris, P.C., Irwin, G.R., 1985. The Stress Analysis of Cracks Handbook, second ed. ASME Press.
Tong, P., Pian, T.H.H., Lasry, S.J., 1973. A hybrid-element approach to crack problems in plane elasticity. Int. J. Numer. Methods Eng. 7 (3), 297–308.
Williams, M., 1957. On the stress distribution at the base of a stationary crack. ASME J. Appl. Mech. 24, 109–114.
Xiao, Q.Z., Karihaloo, B.L., 2003. Direct evaluation of accurate coefficients of the linear elastic crack tip asymptotic field. Fatigue Fract. Eng. Mater. Struct. 26 (8), 719–729.